Indian Geotech J (August 2022) 52(4):753–764
https://doi.org/10.1007/s40098-022-00623-1

ORIGINAL PAPER

Evaluating the Performance of Large-Diameter Bored Piles Socketed in Weathered Rock

Do Huu Dao[1] · Thien Q. Tran[1,2] · Surya S. C. Congress[3] · Anand J. Puppala[3] · Nguyen Minh Hai[4] · Young Sang Kim[5]

Received: 26 January 2022 / Accepted: 28 April 2022 / Published online: 24 May 2022

Abstract The current design practice of the bored piles socketed in rock often ignores the end-bearing resistance and relies only on the side shaft resistance. This is due to the accumulation of soft soils as a result of improper cleaning of the slurry suspension at the bottom of the pile construction. This design practice significantly increases the length and cost of the pile foundation. The current study presents the bidirectional load test results on the large-diameter bored piles socketed in weak rocks at the Cua Dai bridge project, Quang Ngai province, Vietnam. The soil profile consists of medium loose to very dense silty sand underlain by the weathered granite rock. The test results and analyses showed that the ultimate shaft resistance and the maximum end-bearing resistance of the granite rock layer are much smaller than those estimated from the unconfined compressive strength of intact rock. The low shaft resistances are attributed to the presence of the slurry filter cake at the interface between the pile shaft and surrounding rock, while the low toe resistances are due to the presence of the soft soils below the pile toe. The importance of the allowable pile toe settlement and the presence of soft soils below pile toe have been addressed to consider the inclusion of end-bearing resistances in design.

Keywords Bidirectional load test · Shaft resistance · Toe resistance · Weak rocks

✉ Do Huu Dao
dhdao@dut.udn.vn

✉ Thien Q. Tran
tqthien@vt.edu

[1] University of Science and Technology, The University of Danang, Danang, Vietnam

[2] The Charles Edward Via, Jr. Department of Civil and Environmental Engineering, Virginia Polytechnic Institute and State University, Blacksburg, VA, USA

[3] Zachry Department of Civil and Environmental Engineering, Texas A&M University, College Station, TX, USA

[4] Geotechnical and Material Engineering, Testing and Inspection, Riner Engineering, Inc. (RINER), Houston, TX, USA

[5] Department of Civil Engineering, Chonnam National University, Gwangju, Republic of Korea

Introduction

Pile foundation is generally used to bear the vertical loads using skin frictional resistance and end-bearing resistance [1–10]. Many previous studies have discussed the design of the bored piles socketed in rock [4, 11–13]. The current design practice of the bored piles socketed in rock often ignores the end-bearing resistance and relies only on the side shaft resistance. This is due to the accumulation of soft soils as a result of improper cleaning of the slurry suspension at the bottom of the pile construction and also due to the discontinuities in the weathered rocks below the pile toe [14, 15]. This design practice significantly increases the length and cost of pile foundation [16, 17].

To ensure the end-bearing resistance in design, it is necessary to clean the slurry suspension and soft soils accumulated at the bottom of the pile toe to an acceptable level. The thickness of the accumulated soft soil layers must be less than the difference between the allowable settlement of the pile and the elastic shortening of the pile under the design load condition. Including the end-bearing resistance in design, without ensuring this requirement, might result in an excessive settlement of the designed piles and cause damage to the pile-supported structures

[18–21]. This paper presents the bidirectional load test results on the bored piles socketed into the weathered rock layers up to a depth of about 2.5 to 5.0 times the pile diameters and discusses the feasibility of using end-bearing resistances in the pile-supported foundation design for the Cua Dai bridge project, Quang Ngai province, Vietnam.

The Cua Dai bridge is a cable-stayed bridge over the Tra Khuc River in Quang Ngai province, Vietnam. It has an overall length of about 2500 m and accommodates four traffic lanes and two pedestrian footways with a 30-m high navigation clearance for shipping vessels, as shown in Fig. 1. This bridge has four central 120-m spans, two 75-m end spans, supported by 50-m high towers, and thirty-three approach 50-m spans. The foundation of the main bridge pylons and approach structures is placed on the bored piles with diameters of about 1.5 and 1.2 m, respectively. The designed pile depths range from 24.0 to 27.0 m below the river bottom level. The design loads of the 1.2-m and 1.5-m-diameter piles are about 4 and 6 MN, respectively. Basic information of Cua Dai bridge is presented in Fig. 1a-c.

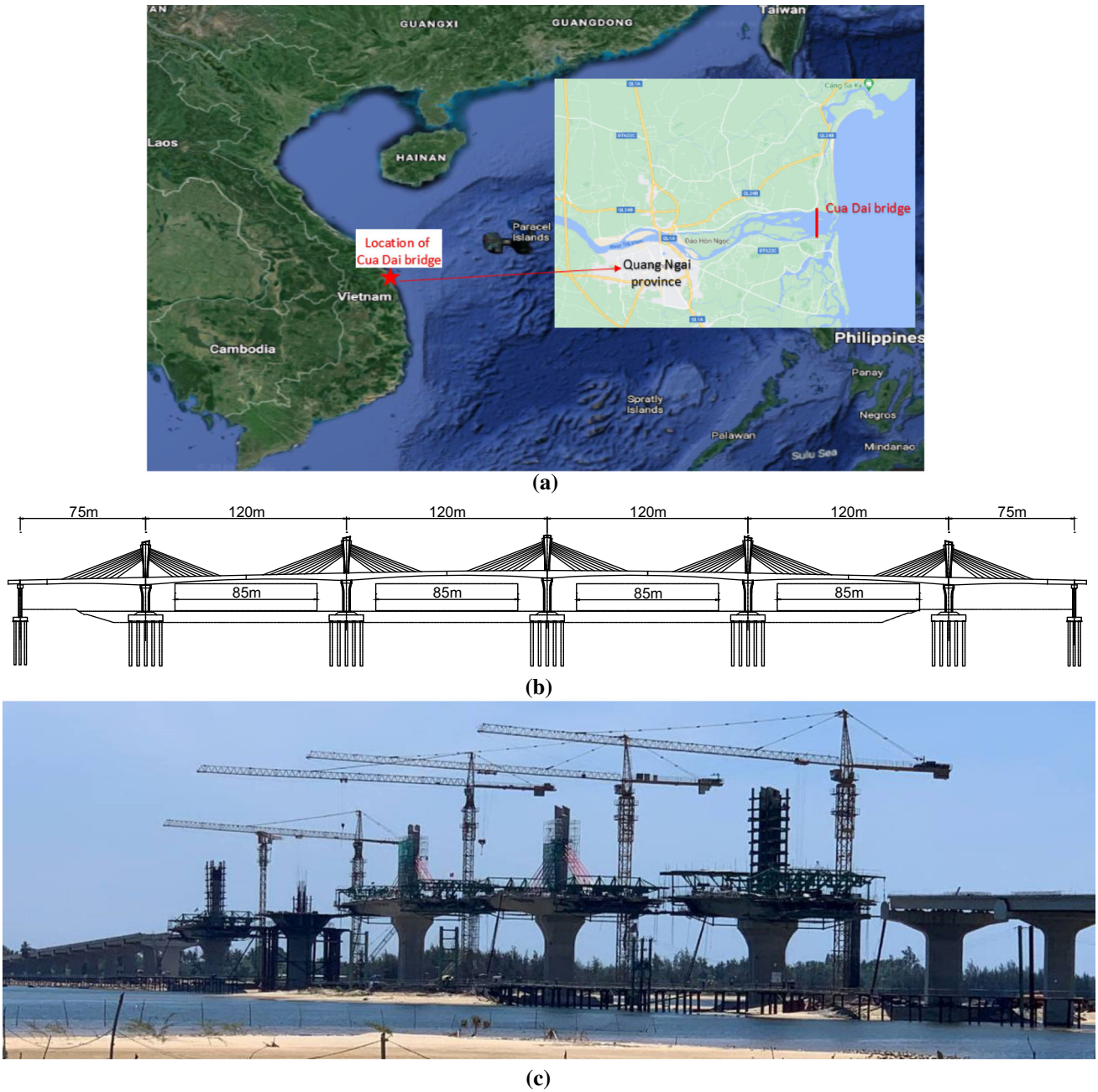

Fig. 1 Basic information of Cua Dai bridge: **a** location of the bridge in Vietnam, **b** design of Cua Dai bridge, and **c** Cua Dai bridge under construction

To assist the pile-supported foundation design of main bridge pylons and approach structures, a bidirectional load test program was performed on four boring piles of 1.2 m and 1.5 m diameters. The soil profile of the project site consists of medium dense to dense silty sand up to a depth of 18 m underlain by the highly weathered granite rock. The depths of the embedded test piles ranged from 24.0 to 27.0 m below the existing river bottom grades. They are socketed into highly weathered granite rock layers up to a depth of about 2.5 to 5.0 times pile diameters. The hydraulic jacks were attached to the steel cages at about 0.5 m above the toe levels of the test piles. To measure the shaft resistances during loading, the 1.2-m and 1.5-m-diameter test piles were equipped with three and four strain gauge (SG) levels, respectively, above the bidirectional cell levels. The bidirectional loading tests were performed after placing concrete for 28 days.

This study presents the results and analysis of the bidirectional loading tests on four bored piles socketed in the highly weathered granite rock layers at the project site of the Cua Dai Bridge, Quang Ngai province, Vietnam. The importance of the allowable pile toe settlement and the presence of soft soils below the pile toe will be addressed to evaluate the feasibility of using end-bearing resistance in pile design.

Soil Characterization

The geological characteristics of the project site obtained from four boreholes (BH1 to BH4) at the four test pile locations (TP1 to TP4), respectively, are shown in Fig. 2.

As shown in Fig. 2, the first soil layer is well-graded sand with 81.5% of soil grains retained on sieve No. 40 (425 μm). Uniformity coefficient (*Cu*) and coefficient of gradation (*Cc*) are 9 and 1.38, respectively. The second soil layer is silty sand with 38% of soil grains retained on sieve No. 40 (425 μm), and 47% of soil grains retained on sieve No. 200 (75 μm), while *Cu* and *Cc* values are 9 and 1.05, respectively. The soil types were classified based on ASTM D2487-06, 2017 [22]. Particle-size distribution of soil layers numbered 1 and 2 is presented in Fig. 3.

The rock layers below the silty sand layers are divided into three sublayers (layers 3 to 5) based on rock quality classification. Total core recovery (*TCR*) and rock quality designation (*RQD*) are the parameters used to classify and evaluate the rock quality at this project site. The *TCR* and *RQD* measurements of rock layer 3 are about 35 and 0%, respectively. This rock layer is highly weathered and is classified as a very poor-quality rock with a thickness of about 3.0 m. Underlying this highly weathered rock layer (layer 3) is the fair-quality rock layer (layer 4) with *TCR* and *RQD* ranging from 58 to 70% and from 50 to 57%, respectively. The 10-m-thick layer 4 is underlain by good-quality granite bedrock (layer 5) with *TCR* and *RQD* measurements ranging from 90 to 98% and 80 to 93%, respectively. The unconfined compressive strengths (*UCS*) of these intact rocks in layers 4 and 5 are about 30 and 35 MPa, respectively. The mechanical and physical engineering properties of the studied soils are shown in Table 1.

Pile Construction and Testing Program

The test piles (TP1 to TP4) were constructed by first inserting casings to about 2 m depth below the existing grades. Then, the shafts were drilled to 24–26 m depths using a bucket drill with bentonite slurry. The drilling equipment was equipped with an artificial diamond-cut edge to penetrate, hard rocks, into the designed depths of the test piles. The bored piles TP1 and TP4 were constructed with a diameter of 1.2 m, while the piles TP2 and TP3 were constructed with a diameter of 1.5 m. As indicated in Fig. 4, the test pile toes were socketed into the fair-quality rock layer of about 2.5 to 5.0 times the pile diameters. In addition, the strain gauges were also attached to each test pile at different levels (SG 1 to SG4) to measure the shaft resistances. They were symmetrically installed along the length of the pile at depths of 7 m, 11 m, and 16 m for pile TP1; 5 m, 9 m, 14 m, and 18 m for pile TP2, 8 m, 12 m, 17 m, and 21 m for pile TP3; 5.5 m, 15.5 m, and 17.5 m for pile TP4. The Geokon 4200 (3000 με) model strain gauges each having a length of 152 mm were used and connected to the observing device Geokon 403 through 4-core cable lines conveying data pertaining to the temperature readings and movements of each pile. The testing piles were cured for 21 days, and then data were collected every 5 min while applying loads.

After drilling completely, the boreholes were cleaned before placing the steel cages. Then, the reinforcing steel cages were lowered into the boreholes with the hydraulic jacks attached to each test pile at about 0.5 m above the designed pile toe levels, shown in Fig. 5. Before placing concrete, the boreholes were re-cleaned to remove the soft soils caused by the installation of the steel cages and the pile test instruments. Three hydraulic jacks were used for each test pile. For the 1.2- and 1.5-m-diameter test piles, the loading capacities of each jack used were about 3 and 5 MN, respectively.

To measure upward and downward displacements of pile segments during loading, the 8-mm-diameter telltale rods placed inside the 21-mm-diameter steel tubes were attached to the steel plates at the top and bottom of the hydraulic jacks. In addition, the 1.2- and 1.5-m-diameter test piles were instrumented with vibrating wire strain gauges installed above the jack levels to measure the shaft

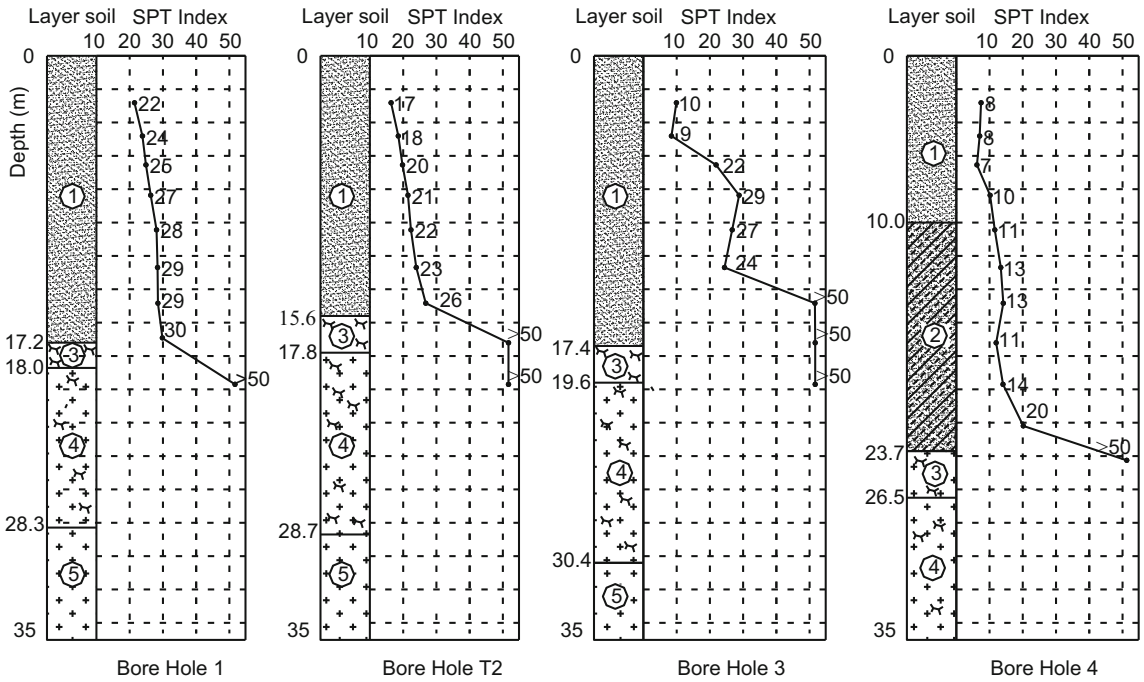

Fig. 2 Soil properties of four bored holes (BH-1 to BH-4) at four test pile locations

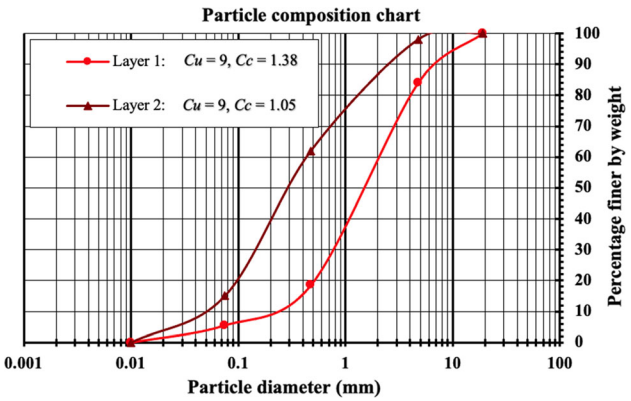

Fig. 3 Particle-size distribution of soil layers numbered 1 and 2

resistance, respectively, as indicated in Fig. 4. The reinforcement used for the 1.2- and 1.5-m-diameter test piles consisted of twenty-five bars of 25 mm diameter and twenty-six bars of 32 mm diameter, respectively. Tubes of 56 and 114mm diameters were also installed for ultrasonic integrity testing and coring testing to check the concrete uniformity and the accumulation of soft soils at the test pile toe during the pile construction, respectively.

The static loading tests were performed after placing concrete for about 28 days (Fig. 5d). The loading procedures were performed by one cycle with twenty equal load increments of 325 and 450 kN until reaching the maximum test loads of 6.5 and 9.0 MN corresponding to 1.2- and 1.5-m-diameter piles, respectively. The unloading was performed by ten equal load decrements for all test piles. The load-holding time periods for each successful load increment and decrement were about 10 and 5 min, respectively. The average compressive strength of 28-day cured concrete cylinders for the test piles was about 30.4 MPa.

Table 1 Physical and mechanical parameters of the studied soil and rock

Layer	Name	Thickness (m)	γ (kN/m^3)	W (%)	W_L (%)	Wp (%)	LI	c (kN/m^2)	φ (Degree)	E_o (MPa)	N_{30}
1	Well-graded sand	10–17.4	19.20	21.6	–	–	–	0	31.1	125.7	8–50
2	Silty sand (BH-4)	13.7	18.64	24.6	30.5	22.4	0.27	0.19	28.1	84.8	10–20
3	Highly weathered rock	1.9–2.2	23.75	RQD = 0%				TCR = 35 (%)		$N_{30} > 50$	
4	Fair-quality rock	8.5–10.9	24.18	RQD = (50–57)%				TCR = (58–70)%		UCS = 30 (MPa)	
5	Good-quality granite bedrock	Below layer 4	24.67	RQD = (80–93)%				TCR = (90–98)%		UCS = 35 (MPa)	

γ unit weight, W water content; W_L liquid limit; Wp plastic limit; LI liquidity index; c cohesion; φ friction angle; E_o elastic modulus; N_{30} SPT counts; RQD rock quality designation; TCR total core recovery; UCS unconfined compressive strength

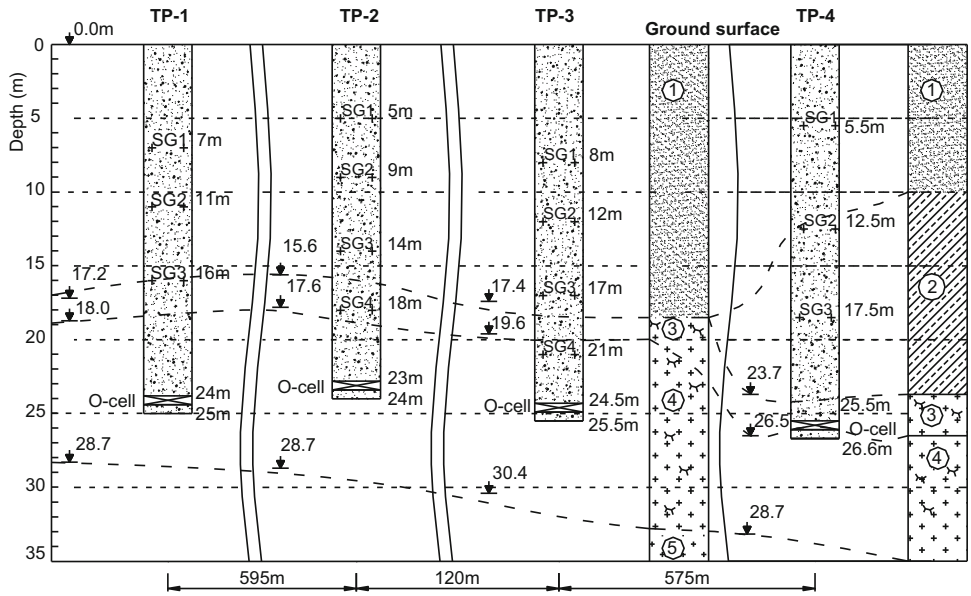

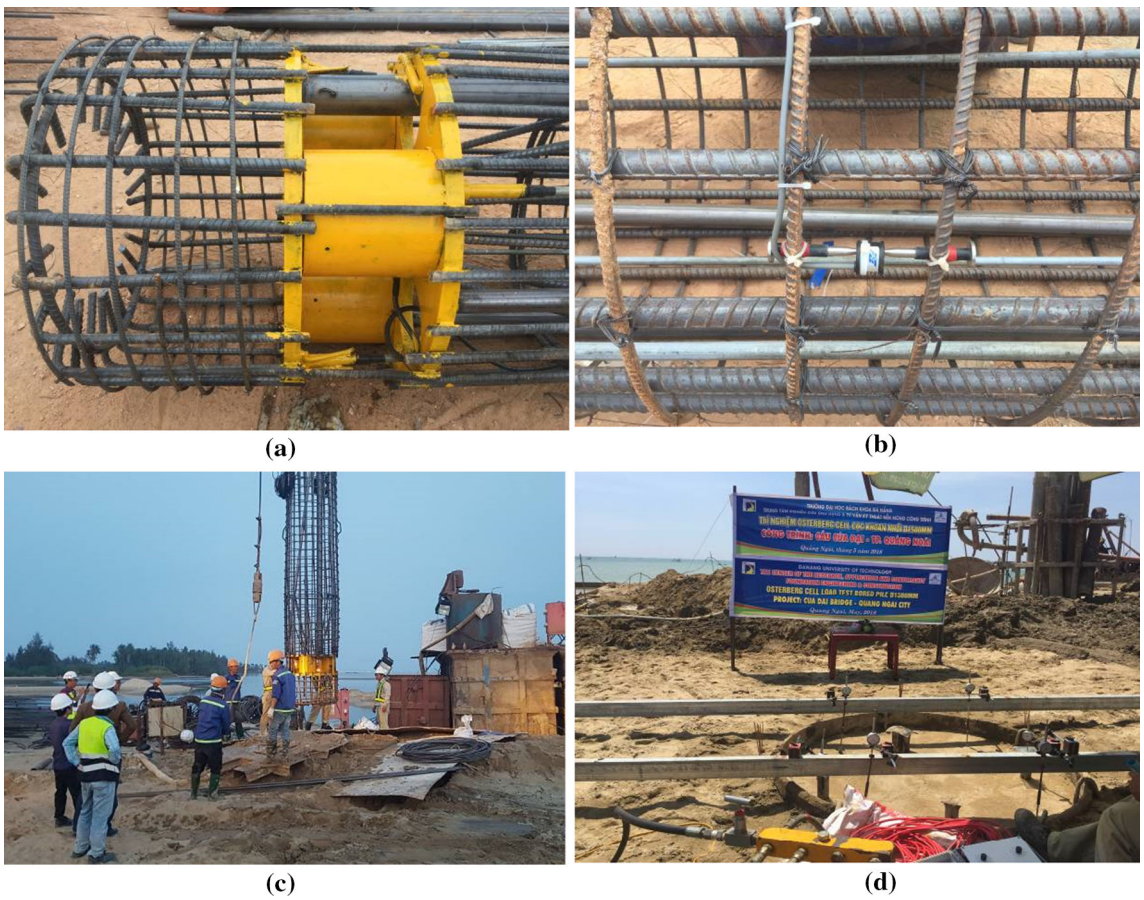

Fig. 4 Pictographic representation of the installed piles and strain gauge levels

Fig. 5 Construction sequence: **a** hydraulic jacks, **b** installation of strain gauges, **c** lowering the steel cage to the drill hole, and **d** static loading tests

Test Results and Analysis

Load Versus Displacement

The measured loads and movements of the four test piles are shown in Figs. 6, 7, 8. The maximum values of the measured loads and movements of the test piles are summarized in Table 2. Under a maximum test load of 6.5 MN for the 1.2-m-diameter piles, TP1 and TP4 (Figs. 6, 7), the maximum downward and upward movements measured at the jack levels were about 7.2 to 7.8 mm and 4.9 to 5.7 mm, respectively. The maximum upward pile head movements were about 1.3 and 0.8 mm for the test piles TP1 and TP4, respectively.

As can be observed from Figs. 6 and 7, the upward and downward load–displacement curves of the pile TP1 are relatively linear, while those of the pile TP4 are significantly steeper. The slope difference of load–displacement curves is attributed to the differences in the rock-socketed pile depths and the soil conditions of these two test piles. As indicated in Fig. 4, the pile TP1 was socketed into the fair-quality rock layer (layer 4) about 5.4 m deep, while the pile TP4 was placed into the very poor-quality rock (layer 3) about 2.3 m deep. The downward load–displacement curve of the pile TP4 has become significantly steeper due to the placement of the pile toe into the weaker rock.

The steeper upward load–displacement curve of pile TP4 is attributed to the presence of the medium dense sandy silt layer (layer 2a) and the loose silty sand layer above the jack installation level. These layers had low SPT-N values ranging from 8 to 20 blows, while the soil profile of pile TP1 above the jack level consists of medium dense silty sands with relatively high SPT-N values ranging from 22 to 30 blows. In addition, the shaft segment of pile TP4 socketed in the rock was about 3 times less than that of pile TP1 as the test pile TP4 was not installed in the fair-quality rock layer (layer 4) as was the case for test pile TP1. This can be seen clearly from the upward and downward load–displacement curves of the test piles TP2

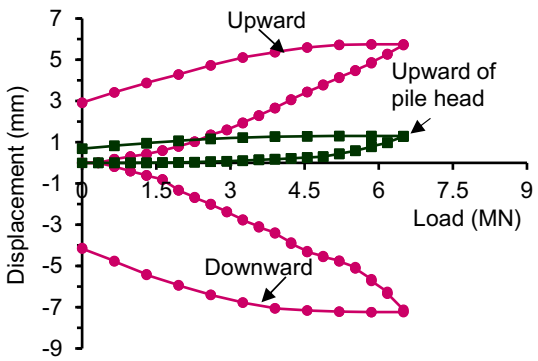

Fig. 6 Load–displacement curves of pile TP-1

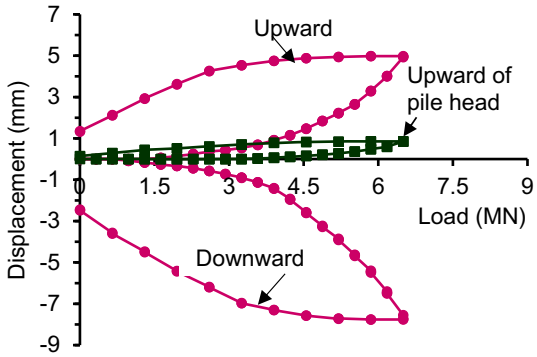

Fig. 7 Load–displacement curves of pile TP-4

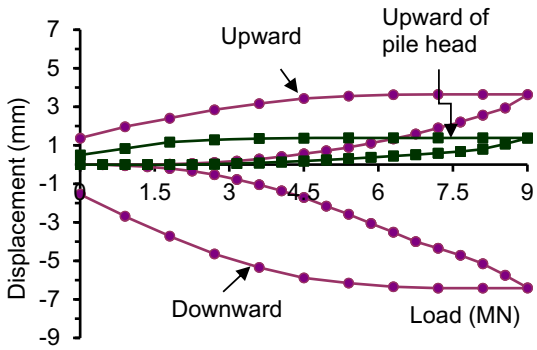

Fig. 8 Load–displacement curves of testing pile TP-2

and TP3 shown in Figs. 8 and 9, respectively. The upward and downward load–displacement curves of these test piles are the same as that of the test pile TP1 due to the similar soil conditions and approximate pile installation depths.

Moreover, it should be noted that the slope of the downward load–displacement curve of the pile TP4 changed dramatically after a load increment of 3.9 MN and this reflects that the shaft resistance of 0.5 m pile segment below the jack level was mobilized completely. The displacement recorded at the loading level of 3.9 MN was about 1.5 mm. In general, the downward load–displacement curves of both test piles exhibited strain hardening and showed no change in the ultimate bearing capacities of the pile toe resistances.

Figures 8 and 9 show the upward and downward load–displacement curves of the 1.5-m-diameter piles TP2 and TP3, respectively. The maximum test loads for these two piles were about 9.0 MN. For this maximum test load, the maximum downward and upward movements recorded at the jack levels were about 4.8 to 6.8 mm and 3.1 to 3.6 mm, respectively. The maximum pile head movements were about 1.4 and 1.1 mm for the test piles TP2 and TP3, respectively. The displacement values of the upper and bottom parts of the loading box and that of the four piles' top are presented in Table 2.

Table 2 Summary of the displacement of testing piles

Testing pile	Max. load (MN)	Max. upward displacement (mm)	Max. downward displacement (mm)	Max. upward pile head displacement (mm)
TP-1	6.5	5.75	7.23	1.31
TP-2	9.0	3.64	6.42	1.39
TP-3	9.0	3.10	4.80	1.15
TP-4	6.5	4.98	7.76	0.86

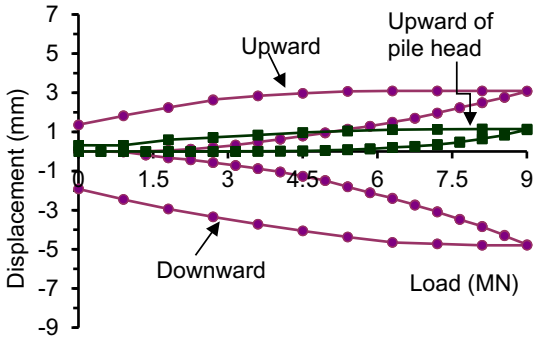

Fig. 9 Load–displacement curves of testing pile TP-3

As mentioned earlier, these two test piles were installed in soil conditions the same as the test pile TP1 with approximately the same pile installation depths. Therefore, the downward and upward load–displacement curves of these piles have relatively gentle slopes similar to those of the pile TP1. For the maximum displacement values and slopes of the downward load–movement curves (Figs. 8 and 9), it can be observed that the soil condition below the pile toe TP3 was better than that of the pile TP2. Improper cleaning of soft soils accumulated at the pile toe TP2 during pile construction might have contributed to this behavior.

Load Distribution

The strain measurements of the vibrating wire strain gauges were collected by using a datalogger during static load tests. The average of strains measured on a cross-sectional area was used to obtain the loads by multiplying it with the stiffness of the pile calculated by the product of elastic modulus and cross-sectional area. The axial force at bored pile cross-section j (P_j) can be obtained using Eq. (1).

$$P_j = \frac{\varepsilon_1 + \varepsilon_2 + \varepsilon_3}{3}(E_s A_s + E_c A_c) \quad (1)$$

where P is the axial load (MN), ε is the strain measured at each cross-sectional area of the bored pile (1, 2, and 3 denote the name of the cross-sectional area), E_s and E_c are the elastic moduli of the steel and concrete (MPa), respectively, and A_s and A_c are the cross-sectional areas of the steel and concrete (m^2), respectively.

Based on the 28-day compressive strength of pile concrete and the reinforcement strength, the average stiffness estimated for the 1.2- and 1.5-m-diameter test piles was about 30.8 and 48.4 GN, respectively. The strains measured at the strain gauge levels were converted into loads based on Eq. (1), and the load distributions along the pile depths for the different loading increments are presented in Fig. 10.

From the load distribution diagrams in Fig. 10, it can be seen clearly that the shaft resistances from the pile head to the gauge levels SG3 and SG4 for the 1.2- and 1.5-m-diameter test piles, respectively, were not mobilized significantly. As opposed to these shaft resistances, the shaft resistances from the jack levels to the adjacent strain gauge levels were mobilized significantly. However, due to these pile segments placed in the weathered rock layers, the load distributions in the pile measured at jack levels were reduced significantly by the shaft resistances of these weathered rock layers. Total shaft resistances of these weathered rock layers ranged from about 73 to 84% and 63 to 72% for the 1.2- and 1.5-m-diameter test piles, respectively.

Mobilized Shaft Resistance

The unit shaft resistance of the test pile was calculated by dividing the difference between the axis loads measured at the level of the jack and the adjacent strain gauge level with the interface area of the pile segments surrounded by soil as shown in Eq. (2).

$$\tau_j = \frac{P_j - P_{j+1}}{\pi D L_j} \quad (2)$$

where τ_j is the side resistance at section j (kPa), D is the pile's diameter (m), and L_j is the length of the pile in soil layer j (m), P_j, is the load measured at section j.

To evaluate the mobilization of the test pile shaft resistances, the calculated unit shaft resistance is plotted against the displacements measured at the jack levels, instead of the displacements at the middle of the pile

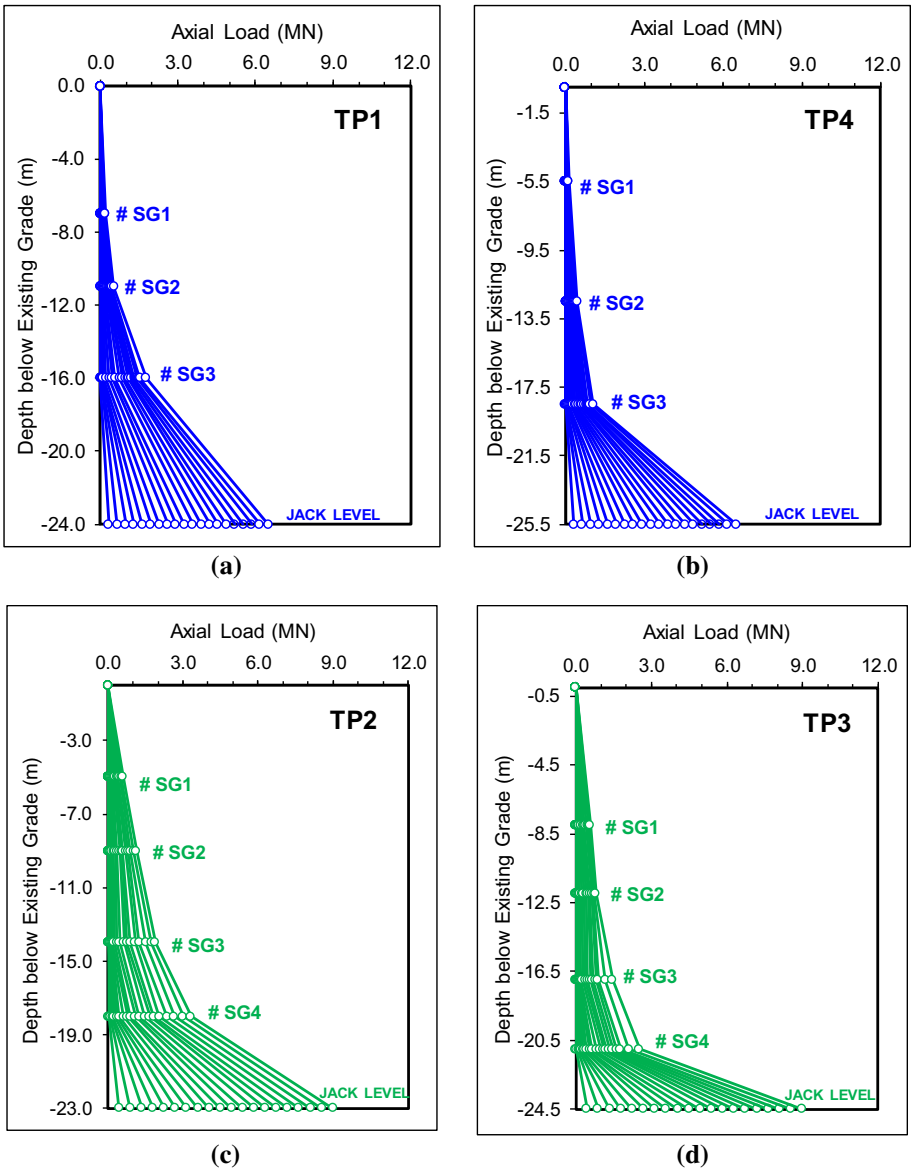

Fig. 10 Axial force distributions of bored testing piles: **a** Testing pile TP-1, **b** Testing pile TP-4, **c** Testing pile TP-2, and **d** Testing pile TP-3

segments. The unit shaft resistance-versus-displacement curves of the four test piles are shown in Fig. 11.

From the unit shaft resistance-versus-displacement curves, it is apparent that only the shaft resistances from the jack installation levels to the adjacent strain gauge levels located at SG3 and SG4 for the 1.2- and 1.5-m-diameter piles, respectively, were mobilized significantly as discussed earlier. In general, once the shaft resistance between the pile and the weak rock has been mobilized fully, the shaft resistance-versus-displacement curve will become a straight line, instead of undergoing strain hardening or strain softening after reaching its peak strength. As can be seen clearly from Fig. 11b, d, the shaft resistances from the jack levels at SG3 and SG4 were mobilized completely. Meanwhile, the shaft resistance-versus-displacement curve of the test pile TP1 from the jack level at SG3 (Fig. 11a) shows the strain hardening, i.e., the ultimate unit shaft resistances were not reached.

As indicated in Fig. 4, the strain gauge levels were installed in the weathered rock layers at SG4 of the test piles TP2 and TP3. However, the strain gauge level SG4 of the test pile TP2 was placed in the very poor-quality rock layer, while that of the test pile TP3 was installed completely in the fair-quality rock layer. Therefore, the shaft resistance of the test pile TP3 was considered as the side shear resistance of the bored pile when socketed in a fair-quality granite rock layer (layer 4), which is about 393 kPa, as shown in Fig. 11d. Many factors are contributing to this low side shaft resistance, such as the shaft wall roughness, discontinuities in the rock mass, shaft geometry, and other factors [16, 17]. Even after considering these factors, the unit shaft resistance measured is still about 2.5 times

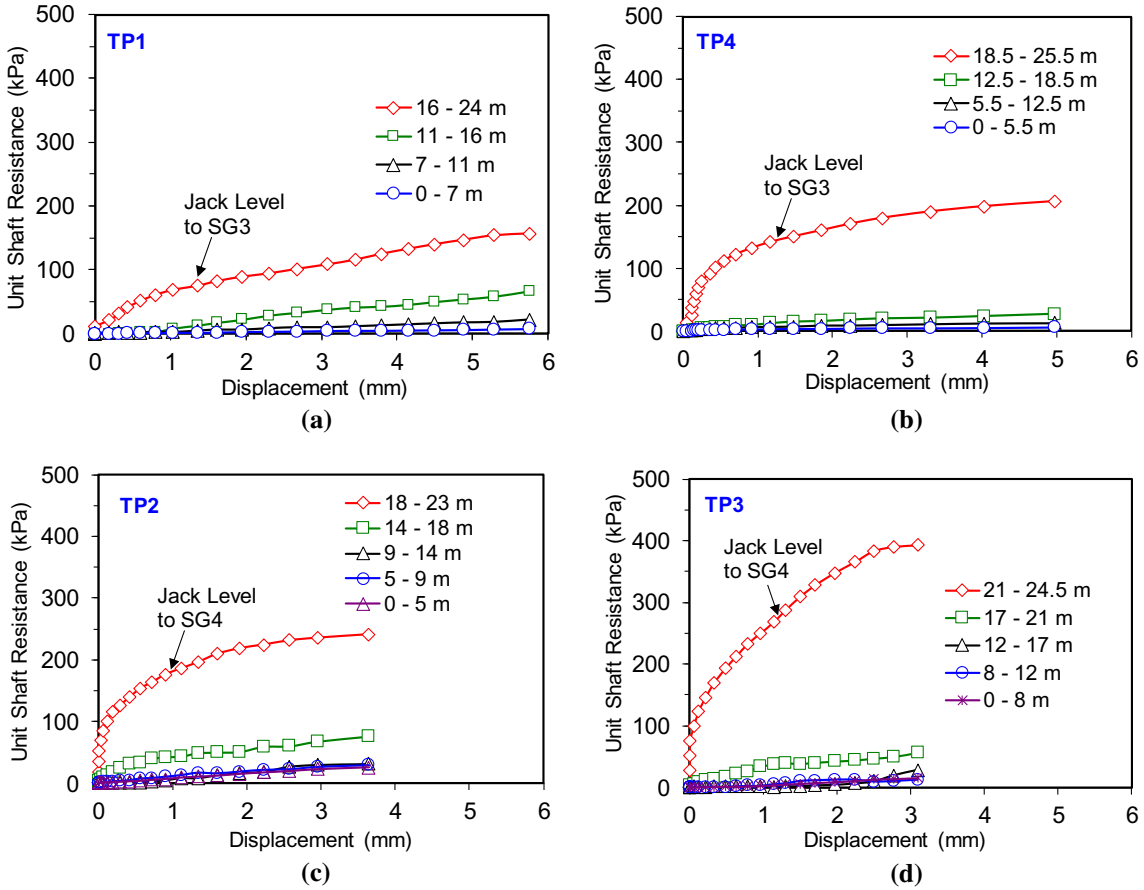

Fig. 11 Relationship between the shaft resistance and the displacement of testing piles: **a** Testing pile TP-1, **b** Testing pile TP-4, **c** Testing pile TP-2, and **d** Testing pile TP-3

smaller than the minimum side shaft resistance of about 30 MPa obtained from the empirical relations for the unconfined compressive rock strength [14, 16, 19]. Therefore, it is likely that the low unit shaft resistance of this pile segment is due to the presence of slurry filter cake at the interface between the pile shaft and surrounding rock.

For the test pile TP2, there are two weathered rock layers (layers 3 and 4) at the level of SG4 with an average unit shaft resistance of about 241 kPa (Fig. 11c), which is about 39% less than the shaft resistance of only layer 4.

As to the 1.2-m-diameter test piles TP1 and TP4, the strain gauge levels were installed in the silty sand (SM) and sandy silt (ML), respectively. Therefore, the average unit shaft resistance-versus-displacement curves of these segments of both test piles are ignored. It was expected that the shaft resistances of the silty sand (SM) and the sandy silt (ML) layers would be obtained from these two test piles. However, due to the smaller test loads, the side shear resistances of the piles at these soil layers were not mobilized significantly as shown in Fig. 11a, b.

Equivalent Load–Displacement Curve

For the field practitioners, it is expected that the load–displacement curves obtained from the bidirectional load tests will be converted into the load–displacement curves of the conventional static load tests. To meet this requirement, an equivalent load–displacement curve construction method was proposed by Osterberg [23]. It was constructed based on three main assumptions: (1) the bored piles are considered as rigid, (2) the upward load–displacement behavior of the shaft resistance of bidirectional test is the same as the downward load–displacement of conventional static load test, and (3) the toe load–displacement behavior of bidirectional test is same as that of the conventional static load test.

The equivalent load–displacement curve construction was performed by selecting several points with similar displacement values in the upward and downward load–displacement curves obtained from bidirectional load tests. Among the points having the same displacement, the loads determined from each curve would be summed and a single point on the equivalent load–displacement curve was then

obtained. By repeating this process for the different displacement points, the equivalent load–displacement curves of the four test piles were constructed and the elastic shortenings of the test piles were also added into the equivalent load–displacement curves after construction, as shown in Fig. 12.

As indicated in Fig. 12, the displacements of the 1.2-m and 1.5-m-diameter test piles are relatively small, only about 2.0 mm for the design loads of about 4 and 6 MN, respectively. The displacements estimated from the equivalent load–displacement curves for conventional static load tests conducted with maximum test loads of 13 and 18 MN corresponding to 1.2-m and 1.5-m-diameter test piles, respectively, are about 10 mm for both cases. In addition, it should be noted that the portions of the excessively equivalent load–displacement curves of the maximum test loads were extrapolated from a hyperbolic function based on the pile test data.

Pile Toe Load–Displacement Curves

Figure 13a, b shows the variation in displacement and normalized displacements for the tip resistance of the 1.2- and 1.5-m-diameter test piles, respectively. From Fig. 13a, it has become clear that the tip bearing capacities of the test piles were not mobilized completely due to the small displacements. In addition, the ratio of displacement to the normalized pile diameters is less than 1%, which is not sufficient to completely mobilize the ultimate tip bearing capacities, as shown in Fig. 13b.

Figure 13a also indicates that the slopes of the tip resistance versus displacement of the test piles TP1 and TP2 have become gentler after the load increments of about 1.5 and 5.0 MN, respectively. These slope changes explain that the soil conditions below these pile tips are relatively soft and it is likely that the cleaning of the boreholes was not done well during the construction of these test piles. Meanwhile, the tip resistance versus displacement of the test pile TP4 is relatively steep at the initial load increments and then it has become gentler after the load increment of about 3.5 MN. As explained earlier, it is likelier that the shaft resistance of 0.5 m pile segment below the jack level contributed to the steepness during the initial load increments of this curve. It is important to note that the tip resistance versus normalized displacement of three test piles TP1, TP2, and TP4 is the same after a load increment of about 5.0 MN (Fig. 13b). Taking everything into consideration, only the tip resistance versus displacement of the test pile TP3 is reasonable to represent the soil conditions of the fair-quality rock layer (layer 4). The observations from the test results of the pile tip coring also confirmed that about 5.0 mm thickness of soft soils was found at the pile tips TP1, TP2, and TP4, while the soil conditions below the pile tip TP3 were the same as those obtained from the soil investigation report. Therefore, to estimate the excessive pile tip loads of the maximum test loads, the test data of this pile were approximated by using the hyperbolic function as indicated by the red curve shown in Fig. 13a, b. This approximated tip resistance versus displacement is useful for considering the developments of the drag loads as well as the changes in the pile foundation design if desired.

To include the end-bearing resistances in pile design, it is necessary to consider the allowable settlement of the designed piles. As stated earlier, the allowable settlement of the pile under the design loads must be less than the sum of the settlement of the soft soil layers accumulated below the pile toe and the elastic shortening of the pile. The elastic shortenings of the 1.2- and 1.5-m-diameter piles estimated are about 3.0 mm while ignoring the effects of the skin friction resistance. It should be noted that the elastic shortenings of piles due to the presence of the side shaft resistances are less than that of the free-standing piles. For the subject case, the allowable settlement of piles

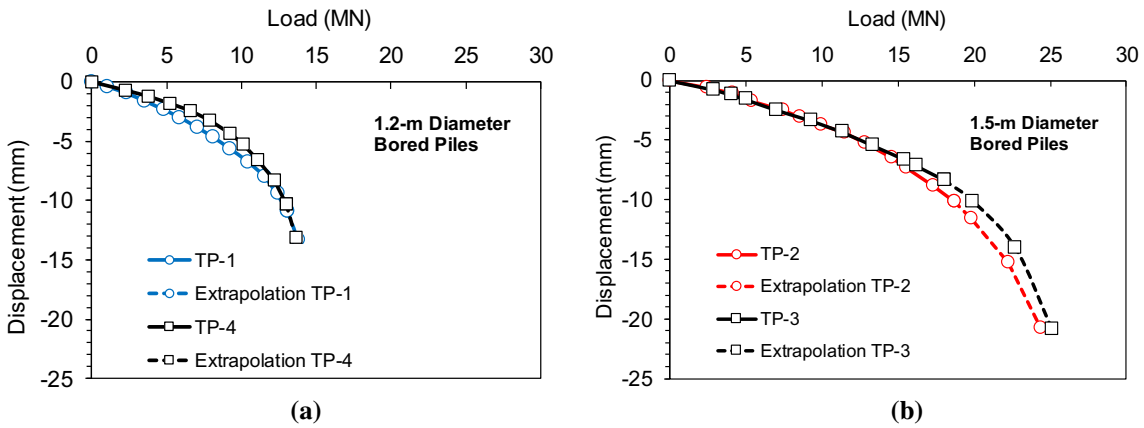

Fig. 12 Equivalent load–displacement curves: **a** 1.2-m-diameter test piles and **b** 1.5-m-diameter test piles

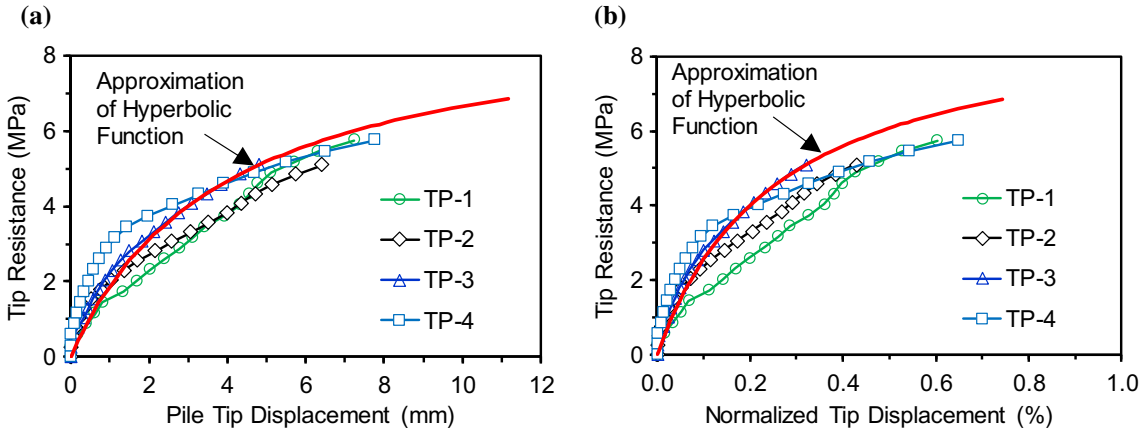

Fig. 13 Hyperbolic functions **a** tip resistance versus displacement of testing piles and **b** tip resistance versus normalized tip displacement of testing piles

is about 10 mm, and therefore the end-bearing resistances determined based on the allowable pile toe settlement of 7.0 mm are about 6.0 MPa (Fig. 13a). This means that the ultimate end-bearing resistances considered to be included in pile design, in this case, are about 6.8 and 10.6 MN for the 1.2- and 1.5-m-diameter piles, respectively.

Based on the unconfined compressive strength of 30 MPa and the average *RQD* of 64% for the rock layer 4, the maximum end-bearing resistances estimated are about 12.9 MPa [16, 17], which is about 2.0 greater that was measured for the allowable pile toe settlement of 7.0 mm. It has become clear that the end-bearing resistance estimated from the unconfined compressive strength of intact rock is not reasonable to be included in design while ignoring the allowable pile toe movements and the presence of the soft soils below the pile toe.

Summary and Conclusions

The bidirectional load tests on the large-diameter bored piles socketed in the weathered rock were performed for the Cua Dai project in Quang Ngai province, Vietnam. The 1.2- and 1.5-m-diameter test piles were constructed to socket into the weathered rock layers of about 2.5–5.0 times pile diameters. The pile test results and analyses were presented. The following conclusions are drawn from these bidirectional load test studies.

- The ultimate side shear resistance of the bored piles in weathered granite rock layers was about 393 kPa, which is about 2.5 times smaller than the value estimated based on the unconfined compressive strength of intact rock.
- The low ultimate side resistances of the bored piles in weathered granite rock layers can be attributed to the presence of the slurry filter cake at the interface between the bored pile shaft and the weathered rock.
- The side shear resistances of the bored pile shaft segments in silty sand and lean silt layers were not mobilized significantly due to the low-test loads.
- The maximum tip resistances of the weak granite rock layers measured are about 6.0 MPa, which is about 2.5 times smaller than the value estimated based on the unconfined compressive strength of intact rock for the allowable settlement of about 7.0 mm.
- The measured pile toe stress–movement curves for the testing piles were strain hardening and showed no toward the ultimate bearing capacities. The toe responses of piles TP1 and TP2 were relatively soft due to the presence of the soft soils accumulated by pile construction and not representative of the pile in weathered granite rock.
- To include the end-bearing resistance in design, it is necessary to determine the allowable pile toe movement and the corresponding end-bearing resistance from the measured test data.
- To assist in considering the development of drag load and the settlement of pile, an end-bearing resistance versus movement curve also has been proposed based on the measured data and the approximation of a hyperbolic function.
- The equivalent load–displacement curves show a displacement of about 2.0 mm under the design loads of 4 and 6 MN for the 1.2- and 1.5-m-diameter test piles, respectively.

Acknowledgements This work was supported by The University of Science and Technology, Da Nang University, Vietnam.

Declaration

Conflict of interest The authors confirm that this article's content has no conflicts of interest.

References

1. Akgüner C, Kirkit M (2012) Axial bearing capacity of socketed single cast-in-place piles. Soils Found 52:59–68. https://doi.org/10.1016/j.sandf.2012.01.012
2. Li H, Liu S, Tong L, Xu X (2018) Investigating the resonance compaction effect on laterally loaded piles in layered soil. Eng Geol 246:1–11. https://doi.org/10.1016/j.enggeo.2018.09.019
3. Li L, Li J, Huang J et al (2017) The bearing capacity of spudcan foundations under combined loading in spatially variable soils. Eng Geol 227:139–148. https://doi.org/10.1016/j.enggeo.2017.03.022
4. Marino G, Osouli A, Zamiran S, Shafii I (2017) Performance of a pier group foundation in swelling rock. Geotech Geol Eng 35:91–109. https://doi.org/10.1007/s10706-016-0087-6
5. Rathod D, Krishnanunni KT, Nigitha D (2020) A review on conventional and innovative pile system for offshore wind turbines. Geotech Geol Eng. https://doi.org/10.1007/s10706-020-01254-0
6. Do H-D, Tran Q-T, Nguyen V-H et al (2021) Performance of foundation on bamboo: geotextile composite improved soft soil in mekong delta through both plate load test and numerical analyses. In: Huang Y-P, Wang W-J, Quoc HA et al (eds) Computational intelligence methods for green technology and sustainable development. Springer, Cham, pp 613–625
7. Dao DH, Hai NM (2018) Lateral loading test results on single and groups of soil-cement columns. 385–393. doi:https://doi.org/10.1061/9780784481592.038
8. Do DHA, Pham T (2018) Investigation of performance of soil-cement pile in support of foundation systems for high-rise buildings. Civ Eng J 4:266. https://doi.org/10.28991/cej-030990
9. Do HD, Pham VN, Nguyen HH et al (2021) Prediction of unconfined compressive strength and flexural strength of cement-stabilized sandy soils: a case study in Vietnam. Geotech Geol Eng 39:4947–4962. https://doi.org/10.1007/s10706-021-01805-z
10. Do HD, Pham VN, Phan CT et al (2020) Full-scale experimental study on the single and group of soil-cement columns under vertical load applying for buildings. Geotech Test J. https://doi.org/10.1520/GTJ20190210
11. Bouafia A (2003) Load-settlement behaviour of socketed piles in sandstone. Geotech Geol Eng 21:389–398. https://doi.org/10.1023/B:GEGE.0000006054.41844.53
12. Omer JR, Delpak R, Robinson RB (2006) A new computer program for pile capacity prediction using CPT data. Geotech Geol Eng 24:399–426. https://doi.org/10.1007/s10706-005-2010-4
13. Yamin M, Khan Z, El Naggar H, Al Hai N (2018) Nonlinear regression analysis for side resistance of socketed piles in rock formations of Dubai area. Geotech Geol Eng 36:3857–3869. https://doi.org/10.1007/s10706-018-0577-9
14. Charles W (2001) Side resistance of large diameter bored piles socketed into decomposed rocks. J Geotech Geoenviron Eng 127:642–657
15. Crapps DK, Schmertmann J (2002) Compression top load reaching shaft bottom: theory versus tests. In: Proceedings of the International Deep Foundations Congress. pp 14–16
16. Zhang L, Einstein HH (1998) Methods of improving the performance of drilled piers in weak rock. J Geotech Geoenviron Eng ASCE 124:574–584
17. Zhang L (2010) Prediction of end-bearing capacity of rock-socketed shafts considering rock quality designation (RQD). Can Geotech J 47:1071–1084. https://doi.org/10.1139/T10-016
18. Doan NP, Park SS, Lee DE (2020) Assessment of Pohang earthquake-induced liquefaction at Youngil-man port using the UBCSAND2 model. Appl Sci. https://doi.org/10.3390/APP10165424
19. Nguyen BP, Ngo CP, Tran TD et al (2022) Finite element analysis of deformation behavior of deep excavation retained by Diagram Wall in Ho Chi Minh City. Indian Geotech J. https://doi.org/10.1007/s40098-022-00611-5
20. Kim YS, Tran TQ, Do TM et al (2018) Preliminary evaluation of the earthquake hazard for underground electric facility lines in Pohang City based on ArcGIS. MATEC Web Conf. https://doi.org/10.1051/matecconf/201820601018
21. Tran TQ, Kim Y, Do TM, et al (2017) Evaluation of the earthquake hazard for underground electric facility lines in Busan area by using Arcgis. pp 57–58
22. ASTM-D2487-06 (2017) Standard Practice for Classification of Soils for Engineering Purposes (Unified Soil Classification System)
23. Osterberg J. (1989) Osterberg method. In: Deep Foundations Institute, Int. Conf. on Piling and Deep Foundations. London, pp 421–427